Received: 15 December 2017 | Accepted: 23 March 2018

DOI: 10.1002/jbio.201700381

Journal of BIOPHOTONICS

FULL ARTICLE

Chylomicrons against light scattering: The battle for characterization

Darya N. Chernova[1,2] | Anastasiya I. Konokhova[1] | Olga A. Novikova[3] | Maxim A. Yurkin[1,2] | Dmitry I. Strokotov[1,4] | Andrei A. Karpenko[3] | Andrei V. Chernyshev[1,2] | Valeri P. Maltsev[1,2,4*]

[1]Voevodsky Institute of Chemical Kinetics and Combustion SB RAS, Novosibirsk, Russia

[2]Novosibirsk State University, Novosibirsk, Russia

[3]Meshalkin National Medical Research Center, Ministry of Health of Russian Federation, Novosibirsk, Russia

[4]Novosibirsk State Medical University, Novosibirsk, Russia

***Correspondence**
Valeri P. Maltsev, Voevodsky Institute of Chemical Kinetics and Combustion SB RAS, Institutskaya 3, Novosibirsk 630090, Russia.
Email: maltsev@kinetics.nsc.ru

Funding information
Russian Science Foundation, Grant/Award Number: 17-75-20117

Chylomicrons (CMs) are lipoprotein particles circulating in blood and transporting dietary lipids. Optically speaking, CMs are small compared to the wavelength of visible light and widely distributed by the size and refractive index (RI). Consequently, intensity of light scattered by the CMs scales with up to the sixth power of their size, hampering simultaneous analysis of 60 and 600 nm CMs. We present an accurate method for quantitative characterization of large-size CM subpopulation by the distributions over size and RI. For the first time the CM characteristics have been determined at a single particle level based on angle-resolved light-scattering measurements. We applied the developed method to 2 key processes relating to CM metabolism, namely in vivo dynamics of CMs in blood plasma after a meal and in vitro lipolysis of CMs by the lipoprotein lipase in post-heparin plasma. We have observed the substantial variations in CM concentration, size and RI distributions. This opens the way for a multitude of medical applications involving screening of CM metabolism, which we exemplified by revealing large differences in CM characteristics after a 12-hour fast between a healthy volunteer and a patient with atherosclerosis.

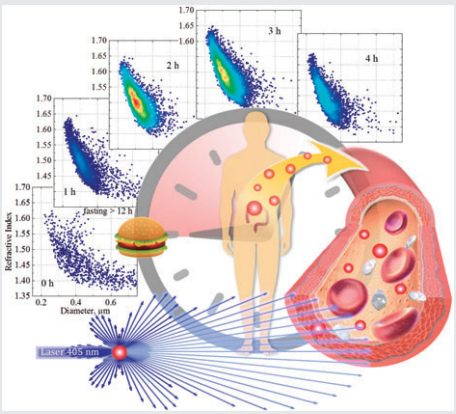

KEYWORDS
characterization, chylomicrons, flow cytometry, light scattering, lipolysis

1 | INTRODUCTION

Chylomicrons (CMs) are lipoproteins that transport dietary lipids and fat soluble vitamins from the intestine to tissues expressing lipoprotein lipase (LPL) [1]. CMs belong to the largest type of lipoprotein particles (typical sizes from 70 to 600 nm) [2, 3], they are spherical in shape and consist of triglycerides (TG) (85%-92%), phospholipids (6%-12%), cholesterol (1%-3%) and proteins (1%-2%) [4]. After food intake, that is, in postprandial state, CMs in blood become larger and their number increases, producing peak of the TG concentration after 3 to 4 hours and slowly returning to the baseline after 6 to 8 hours [5, 6]. After lipolysis (hydrolysis) by the LPL, CMs are reduced in size and become CM remnants, which continue to circulate until taken up by the liver. The half-life of individual CMs is normally 5 to 10 minutes [7, 8], while it takes approximately 10 to 12 hours to clear the blood of CMs after a meal [9].

The increased fasting concentration of CMs in blood indicates its impaired removal. This can be caused by a number of genetic disorders [10] or correlated with overweight and obesity [11, 12], as well as with the metabolic syndrome [13]. It has also been also considered as one of the factors in the development of atherosclerosis [14–16]. Despite clinical evidence that postprandial lipemia, that is, large concentrations of CMs and TG-rich remnant particles, including CM remnants and very low density lipoproteins (VLDL), can contribute to atherosclerosis, the exact mechanisms of such processes are unknown [17, 18]. Both large variability of CMs under physiological conditions and their potential clinical (or diagnostic) significance motivates the development of methods for characterization of CMs in blood plasma.

The simplest qualitative analysis is commonly performed by separating CM fraction using density gradient, sequential ultracentrifugation, or standing plasma test based on differences in the density of lipoprotein fractions (with CMs associated with density $\rho < 1.006$ g/mL) [19, 20]. Alternatively, lipoprotein electrophoresis on agarose gel can be used [19]. By contrast, quantitative metabolic CM assays imply estimation of concentration of CM particles indirectly through determining TG and apolipoprotein B-48 levels in blood serum using immunoblotting or ELISA assays [21, 22], also with combination of sequential flotation ultracentrifugation [23]. However, TG carried by the VLDL and their remnants also heavily contribute to the total TG concentration in plasma [5], whereas apo B-48 protein is present on CM remnants as well. Moreover, such assays provide no information about characteristics of individual CMs such as shape, size, and density.

Historically, the first direct observations of CMs and estimation of their sizes were performed with dark-field microscopy in the size range 0.5 to 1 μm [24]. Due to the small size of CMs and diffraction-limited resolution, optical microscopy was further replaced by electron microscopy to enable the measurement of the complete size distribution of these lipoproteins. In particular, the electron microscopy in combination with ultracentrifugation was used to size CM in the range from 75 to 450 nm [2]. Still, harsh sample preparation and weak statistics restricted usage of electron microscopy for routine characterization of CMs paving the way for more user-friendly methods.

The common option is the dynamic light scattering (DLS) [25–29]. It was applied to lipoprotein particles and resulted in the distribution with 2 peaks: 100 to 140 nm for small lipoprotein particles, and 330 to 350 nm for CMs [26]. However, this method has some serious limitation in the study of disperse systems. First, fundamentally the DLS determines only the hydrodynamic diameter of particles, and absolute concentration can only be determined if the particle is assumed to be a homogeneous sphere with known refractive index (RI). In particular, variation of RI with size, or even a broad distribution of RI independent of size leads to uncontrolled skewing of the measured size distribution. In case of solvation or presence of a stabilizer shell, the apparent density (or RI) and the hydrodynamic diameter will be smaller and larger, respectively, than that of a particle core [30, 31]. Second, DLS is inherently limited by the dynamic range of the detectors, which is especially problematic in the range of CM sizes (smaller than the wavelength), where the light-scattering intensity scales with the sixth power of size [32]. Thus there is a need for a high-throughput method to characterize CMs at single particle level.

The scanning flow cytometry (SFC) is a promising method for such detailed and accurate characterization, since it provides measurement of light-scattering patterns (LSPs) of single particle in a flow [33, 34]. The characterization is performed through the solution of the inverse light-scattering (ILS) problem, given an appropriate particle shape model. This was successfully demonstrated for different blood cells [35–37] and, recently, for microparticles in blood plasma [38, 39]. In the latter studies the LSP measurements were combined with conventional forward and side scattering (FSC and SSC), resulting in sub-diffraction precision of microparticle sizing (about 20 nm) and a few thousandths precision in RI estimates. Part of the measured microparticles was actually CMs [39], but this classification has not been discussed in details.

In this paper, we specifically focus on CMs with the goal to fully reveal the potential of the SFC for their analysis. Supplementing the previously developed solution of the ILS problem, we develop a quantitative method to characterize the whole CM population. Given the complete description of the SFC detection function, we reconstruct the right tail of the CM size distribution and fit it with either exponential or gamma distribution. We test our characterization method during the key processes of CM metabolism, namely, in vivo postprandial dynamics of CMs in blood plasma during 5 hours after a meal and in vitro CMs lipolysis. We also hint toward diagnostic potential of the method by comparative analysis of CMs in a healthy volunteer and a patient with atherosclerosis.

2 | MATERIAL AND METHODS

2.1 | Subjects

The study was approved by the local ethics committee of Meshalkin National Medical Research Center. Informed consent was obtained from all participants of this study, including 2 healthy volunteers and a patient diagnosed with atherosclerosis. All subjects were asked to fast overnight for more than 12 hours prior to the studies.

2.2 | Blood plasma preparation and measurements

Blood samples were collected in 4.5-mL BD Vacutainer sodium-citrate (0.105 M, 3.2%) tubes (Becton Dickinson,

Plymouth, UK). Plasma was obtained by natural precipitation within 2 hours of the collection. Ten microliter of supernatant were diluted 300-fold in 0.2 μm filtered (Sartorius Stedim Biotech GmbH, Goettingen, Germany) buffer containing 0.9% saline with preliminarily added 0.7 and 2 μm reference polystyrene (PS) microspheres. Two hundred microliter of aliquots was used to perform an analysis of single CMs in blood plasma using the scanning flow cytometer (SFC). The dilution buffer was additionally analyzed between measurements for contamination by foreign particles with size and RI falling within the CM ranges; their concentration did not exceed10^{10} L^{-1}.

A volume of 4.0-mL BD Vacutainer serum tubes (Becton Dickinson, Plymouth, UK) were used in dynamic studies for blood collection to measure total plasma TG by enzymatic methods (Triglyceride Reagent, OSR60118, Beckman Coulter, California).

2.3 | Postprandial dynamics of CMs in blood

An intravenous sampling cannula was placed in a cubital vein of a healthy volunteer. Blood samples for CM analysis by the SFC were drawn either in fasting state (after 12 hours fast) or during 5 hours (with 30 minutes intervals) after the volunteer consumed a high-fat breakfast. Blood samples for total plasma TG analysis were also drawn in the fasting state and during the same 5 hours after a meal with 1 hour intervals.

2.4 | CM lipolysis by the lipoprotein lipase during the incubation with postheparin plasma

Pre- and post-heparin blood was drawn from a fasting healthy volunteer before and 15 minutes after intravenous injection of heparin (100 units/kg of body weight). LPL-rich plasma was obtained by centrifugation of postheparin blood for 60 minutes at 4000*g* and 4°C. The volunteer consumed a high-fat breakfast 30 minutes after the heparin injection, and CM-rich blood sample was collected 3 hours after the meal.

Lipolysis of CMs was initiated as follows: 200 μL of postprandial CM-rich plasma was mixed with 200 μL of LPL-rich postheparin plasma and 200 μL of 0.2 μm filtered 0.9% saline containing 2.5% fatty acid-free bovine serum albumin.

2.5 | Scanning flow cytometer

Technical features of the SFC were described in detail elsewhere [33, 34]. The current configuration of the SFC was fabricated by Cytonova LLC (Novosibirsk, Russia). It measures angle-resolved light scattering in a form of the LSP for individual particles using a 405-nm laser (30 mW, Radius, Coherent Inc., Santa Clara, California), which beams parallel to the cell flow, and the original light collection system. The 488-nm laser (15 mW laser, FCD488-020, JDS Uniphase Corporation, Milpitas, California) is used to produce forward (FSC) and side scattering signals (SSC) in a conventional manner [39]. The operational angular ranges in which SFC measures light-scattering information (angle-resolved LSP, FSC and SSC) were determined for each experiment from analysis of 2 μm PS microspheres for the LSP and analysis of a mixture of different PS microspheres for the FSC and SSC, as described previously in [35, 39], respectively.

2.6 | Identification and characterization of individual plasma particles

Flow cytometric analysis of platelets and other plasma constituents, including CMs, in blood samples obtained without centrifugation, washing, or other impacting preanalytical steps, on the basis of their forward- and side-scatter signals alone is a challenge [40]. We chose to follow this path in order to avoid platelet activation accompanied by expression of submicron particles, which can have similar size and RI to that of CMs. We distinguish platelets and CMs on the basis of LSPs measured for individual particles, using the 2-stage characterization algorithm previously developed for label-free identification of microparticles in platelet-rich plasma [38]. According to it, at the first stage platelets are separated from other plasma components on the basis of the forward part of their LSP and the particle size, determined from the solution of the ILS problem assuming the shape of an oblate spheroid [36].

The remaining part of detected plasma particles, including CMs and, possibly, cell-derived microvesicles, seem to be mostly spherical [41, 42]. We applied the Mie theory to fit their LSPs, FSC and SSC amplitudes as described in [39]. Thus, we identify and characterize individual CMs in platelet-rich plasma by their spherical shape, size, and RI from the solution of ILS problem and construct distribution of CM population over these characteristics (see Figures 1 and 2). Uncertainty estimates of determined particle characteristics served as a criterion to control applicability of the Mie theory and, thus, the deviation of the particle shape from a sphere. To remove strongly non-spherical or noisy events from further consideration, we excluded particles with extremely high values of RI ($n > 1.68$) or with the number of intersections of experimental and best-fit theoretical LSPs less than 10 (the LSPs are discretized into 101 points). The latter was first proposed in [43] to distinguish spherical and non-spherical events, attributing the latter to "not-identified" plasma events, including cell fragments, particle aggregates, etc.

2.7 | Instrument detection function

Unfortunately, a large part of CMs has scatter intensity below the SFC detection limit, which is, in general, determined by threshold levels of the SFC optical channels. For current SFC configuration the limiting factor is the FSC channel used to detect single particles within a SFC measurement zone and to trigger instrument electronics. This triggering is based on a

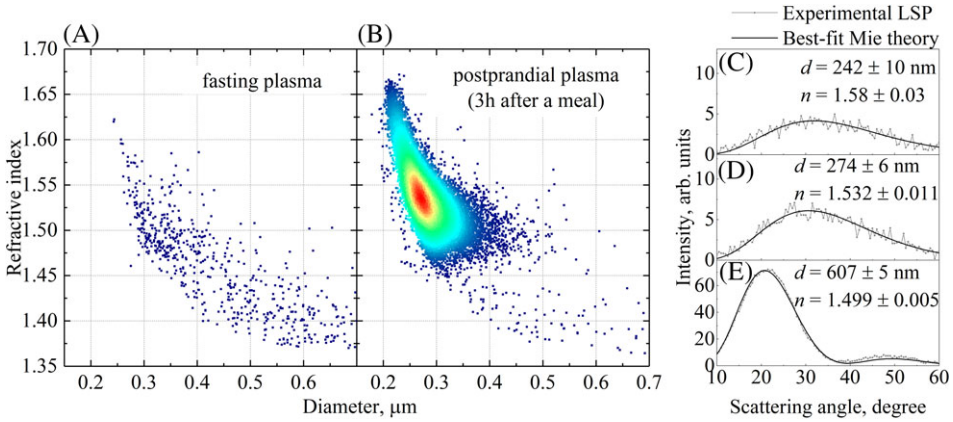

FIGURE 1 (A) and (B): maps of RI vs diameter for spherical submicron plasma particles, identified in PRP of a healthy volunteer, isolated after more than 12 hours fasting and 3 hours after a meal. Here and in the later figures the color indicates the local density of points, normalized by the measured sample volume to facilitate direct comparison in terms of particle concentrations. (C-E): Typical results of the solution of the ILS problem for experimental LSPs of CMs from (B), depicting weighted experimental and best-fit theoretical LSPs (based on the Mie theory). Estimates of particle diameter d and RI n are also shown (mathematical expectation ±SD)

fixed threshold level, against which the signal is compared for each time point independently, in contrast to Gauss-fit that is used on a later step to accurately calculate the single FSC amplitude (discussed above). Since the FSC signal occupies only several time samples of the analog-to-digital converter and signal-to-noise ratio may be small, the detection is a random event even if the particle itself is fixed. The instrument detection function is, by definition, this random probability $F_{\text{det}}(d,n) = \Pr\left(\exists t : I^{\text{FSC}}(t|d,n) \geq I_0^{\text{FSC}}\right)$, which depends on the size and RI of the underlying particle. In order to determine this function we simulated experimental FSC signals as Gaussian peaks with added white Gaussian noise. Width of peaks, SD of experimental noise, and amplification coefficient of the FSC detector were determined from the experimental signals. Peak amplitudes were calculated using Mie theory given the collection solid angle for the detector. Typical experimental and simulated FSC signals are shown in Figure S2A in the Supporting Information.

Thus, we calculated the instrument detection function $F_{\text{det}}(d,n)$ over the grid 250 × 100 for the size and RI, respectively, varied within the ranges of CMs characteristics: $d \in [0.1; 1.2]$ and $n \in [1.35; 1.7]$. An example of 3D representation of this function corresponding to observations of dynamics of CM lipolysis in postheparin plasma is given in Figure S2B, while the 2 constant levels of detection probability (0.1 and 1) are depicted in Figure 2A. The same constant levels are shown in Figure S3 depicting the differences between the SFC detection efficiencies determined for observations of CM lipolysis and postprandial dynamic, performed under different experimental (instrumental) conditions.

2.8 | Characterization of the whole CM population

Since the instrument sensitivity allows us to detect and measure only a limited larger-sized part of the CM population, it is a challenge to even classify the type of the underlying

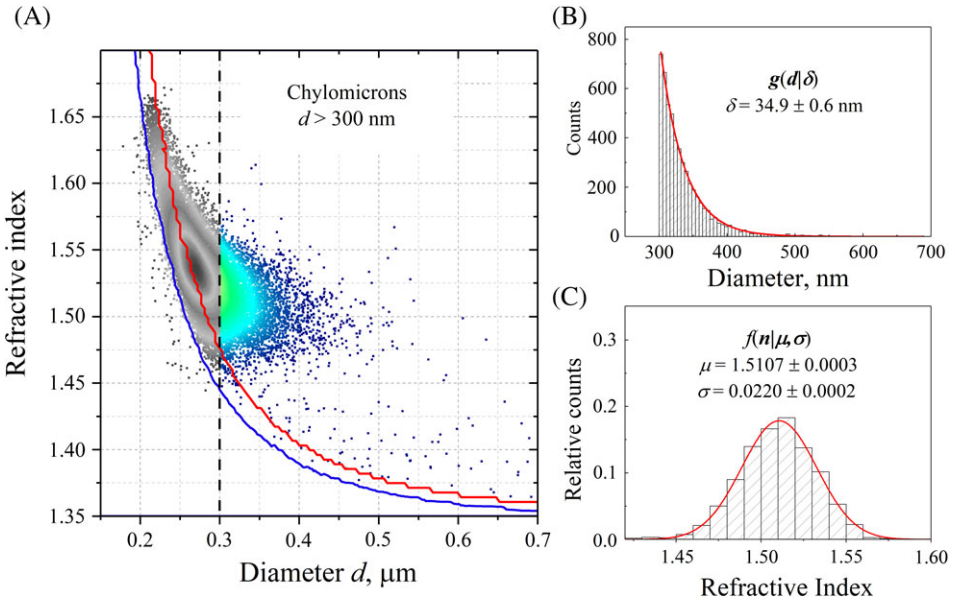

FIGURE 2 (A) Dot-density map representation of size and RI of CMs, detected by the SFC: colored curves represent upper limits of areas with detection probability $P < .1$ (blue) and $P < 1$ (red). Only CMs lying to the right of the vertical dashed black line (with $d > 300$ nm) are further processed to construct and characterize measured CM distributions over size and RI. (B) Reconstructed CM size distribution fitted by exponential distribution with the scale parameter δ. (C) Gaussian fit of CM distribution over RI and best-fit distribution parameters: μ (mean) and σ (SD)

distribution of CM over the size and RI. Moreover, direct characterization of the measured CM population by such statistical quantities, as mean, median, SD, etc., makes little sense due to large differences with that of the underlying whole-population distribution and its dependence on specific experimental conditions. While we can accurately describe the SFC detection function (see Section 2.7), it is still a problem to incorporate uncertainty of size and RI estimates for individual particles, which significantly increases with decreasing particle size. The latter is especially pronounced for the accuracy of RI estimates upon approaching the SFC detection limit and requires a complex mathematical treatment, which we leave for future research. In this paper we limit ourselves to CMs with $d > 300$ nm (for most of experiments), which has good accuracy of individual particle characterization and distribution over RI, which is only slightly distorted by uncertainties and the curved SFC detection limit. In particular, it is reasonable to assume that the RI distribution for this truncated subpopulation is independent of the size and can be described by the normal distribution:

$$f(n|\mu,\sigma) = \frac{1}{\sqrt{2\pi\sigma^2}} \exp^{-\frac{(n-\mu)^2}{2\sigma^2}}, \quad (1)$$

parameterized by mean μ and SD σ (see Figure 2B).

The only exception is the observations of CM postprandial dynamics, for which we increased the size threshold to 350 nm due to the abovementioned differences in experimental conditions. The increased signal-to-noise ratio in both FSC and LSP channels for these experiments resulted in the reduced SFC detection efficiency (Figure S3), deteriorated accuracy (Figure S4), and increased correlation of particle's size and RI estimates. This made the assumption of RI distribution of truncated CM subpopulation ($d > 350$) being independent of the size unrealistic. Thus, in this case we switched to characterization of RI of CM population considering all detected particles.

It is hard to overstress that the size-truncated subpopulation is even less representative of the whole CM population than all detected CMs. However, it is the one with well-controlled accuracy and exactly corresponds to the right tail of the underlying CM size distribution (Figure 2A). In other words, we selected the subset of the data which can be rigorously processed without too much mathematical complexity. Given the probability distribution of CMs over RI, we obtain the marginal (size-dependent) detection function $F_{\text{det}}(d)$ by integrating $F_{\text{det}}(d,n)$ weighted by $f(n|\mu,\sigma)$ over the whole range of n. Dividing truncated experimental size distributions by this detection probability (see Figure S5), we reconstruct size distribution of CMs within the selected size range ($d > 300$ nm or d > 350 nm) to further fit them by any model. The reconstruction step is especially important, when the whole CM distributions shifts to the lower RI upon the action of LPL (Figure 3, see also Figure S6).

While we observe only the tail of the CM size distribution, this tail happens to be remarkably linear in logarithmic scale for all our measurements (a single example is given in Figure S7A, other data not shown). The discrepancies at the largest sizes are causes by statistical noise (counts are less than 10). Therefore, it is natural to fit this tail by the exponential distribution:

$$g(d|\delta) = A\exp^{-d/\delta}, \quad (2)$$

characterized by amplitude A and scale parameter δ. Importantly, δ has a clear meaning in terms of the whole CM size distribution—it is the scale parameter of its exponential tail.

The drawback of such simple exponential decay is that attempts to extract any additional information are expected to be futile. For instance, a natural extension of the exponential distribution is the gamma distribution, which probability density is:

$$g(d|\tau,\delta) = Ad^{\tau-1}\exp^{-d/\delta}, \quad (3)$$

having 1 extra parameter τ. Apart from the exponential tail it also has physically desirable bell shape; thus we tried to fit it to our data (Figure S7B). As expected, the visual quality of fit is the same as for the exponential model and τ is determined with very bad accuracy (mean value 7, SD 4); considering the 95% confidence interval we can only limit its value

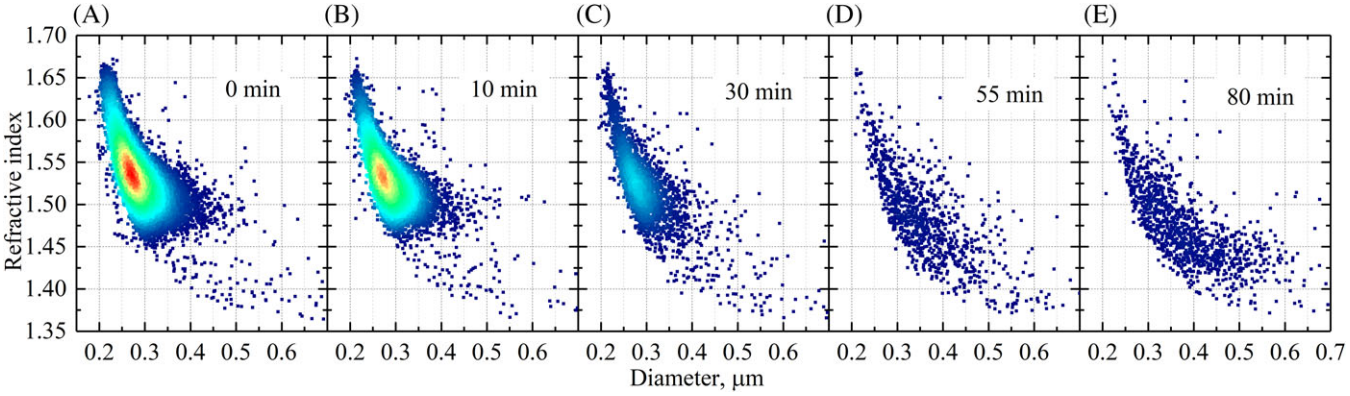

FIGURE 3 Dynamics of size and RI of CMs undergoing lipolysis by the lipoprotein lipase during incubation of CM-rich postprandial plasma (3 hours after a meal) with LPL-rich postheparin plasma at $T = 37°$. Parts (A) to (E) depict dot-density maps of RI vs diameter, measured after 0, 10, 30, 55 and 80 minutes of the incubaion, respectively

from above. Due to that the shown best-fit distribution is only one probable option, and we cannot extract any reliable information about the mode position (see also the confidence band in Figure S7B. The estimate of δ can be considered satisfactory and consistent with that of exponential distribution, since it is mostly determined by the tail. However, its uncertainty is 10 times larger, which motivates us against using the gamma distribution in the production algorithm.

Using other standard distributions is even less meaningful. For example, seemingly obvious log-normal distribution can, in principle, fit the exponential tail. However, the decay rate depends on both parameters of this distribution, thus none of them can be determined with a satisfactory accuracy.

3 | RESULTS AND DISCUSSION

3.1 | Characterization of individual CMs in fasting and postprandial plasma

We analyzed submicron plasma particles in fasting and postprandial plasma of a healthy volunteer, collected 3 hours after a meal. LSPs, SSC and FSC scatter intensities of individual particles were measured with the SFC. Size and RI for each detected particle were determined from the solution of the ILS problem by fitting scatter measurements using the Mie theory. Results of particle characterization in the fasting and postprandial plasma are shown in size-RI dot-density maps in Figure 1A,B, respectively. As compared to the fasting sample (Figure 1A) the postprandial plasma demonstrates a significant growth in particles with RI values close to that of lipids (Figure 1B), allowing one to assume that the majority of them are CMs, known to mainly consist of triglycerides (86%-92%) [44], which RI ranges from 1.441 to 1.491 (at wavelength 434 nm) [45]. Diameters of these particles, not exceeding 500 nm, also fall within the range, typical for this type of lipoproteins. Small fraction of sphere-like particles detected in the fasting plasma can be attributed to residual CMs, whereas a minor part of particles with relatively small RI values (<1.45) probably relate to cell-derived microvesicles or CMs, which underwent partial lipolysis and lost part of their TG content.

Typical results of single particle characterization (solution of the ILS problem) for CMs are shown in Figure 1C-E, depicting experimental LSPs, best-fit theoretical simulations, and determined particle characteristics, including size and RI, together with uncertainties.

3.2 | Characterization of a whole CM population in plasma

Since the final goal is to characterize the whole population of CMs in plasma samples, for example, by its distribution over size and RI, the simplest way is to plot individual particle characteristics as a map over these characteristics, as in Figure 1A,B, or represent them as histograms and use descriptive quantities, such as mean, median, SD, etc. However, the latter approach cannot be easily applied to characterize CMs, measured by the SFC, since the instrument sensitivity allows detecting and characterization of only a larger-sizes tail of the entire CM population. The instrument detection area is a curved region in coordinates of size and RI, which is discussed in details in Section 2. Importantly, the detection threshold is not a single sharp boundary, but is smoothed according to the variation of the detection probability from 0 to 1. For example, the region to the right of the red curve in Figure 2A, which contains the apparent peak of measured CM distribution over size and RI, corresponds to the 100% SFC detection efficiency. Probability to detect single CMs under this curve rapidly decreases with decreasing size and/or RI and does not exceed 10% after crossing the blue curve. Hence, the statistical quantities derived from the measured size and RI distributions generally depend on the particular optical configuration of the instrument and size-to-noise ratio of its channels.

To alleviate the instrument dependence one can try to reconstruct the 2-dimensional size-RI distributions of the entire CM population on the basis of truncated measured data. However, potential solution of this problem requires not only realistic models of the entire size-RI distribution (not known in the literature) and of the detection function (described above), but also the complete understanding of all factors leading to non-uniform distortion and broadening due to the uncertainties of individual measurements. For instance, apparent broadening of particle distribution over RI with decreasing particle size in Figure 1 is caused by substantial decrease of accuracy of individual RI estimates (Figure 1C-E), hiding their natural variability by composition. Despite our ongoing progress in estimating uncertainties of single measurements (see Section 2), the rigorous model similar to that of the detection function is still lacking.

Facing the described uncertainties, we chose a rigorous analysis of a part of data over an approximate analysis of the whole dataset. In particular, we further process only CMs with size $d > 300$ nm for which the distribution is distorted by the SFC detection limit and uncertainty of ILS problem to the least extent (Figure 2A). In other words, size and RI uncertainties (median values are 4 nm and 0.006, respectively) are small enough to be neglected, while thresholding the size alone effectively reduces the analysis of distributions to the 1-dimensional 1. It should be additionally noted that the specified size threshold (300 nm) depends on specific experimental conditions and may vary between observations. Finally, we reconstruct the truncated size distribution, taking into account the instrument detection function as described in the Section 2, and fit it by the exponential distribution defined by Eq. (2) and characterized by

amplitude A and scale parameter δ (Figure 2B). RI distribution is described by the normal distribution defined by Eq. (1) (Figure 2C).

3.3 | Lipolysis of CMs in LPL-rich postheparin human plasma

Prior to the investigation of the dynamics of CM characteristics under the action of the LPL during the incubation with postheparin plasma, 3 plasma samples, including pre- and post-heparin fasting plasma and postprandial plasma, were analyzed for CM content using the SFC and for total plasma TG levels using a standard colorimetric assay.

TG levels in pre- and post-heparin fasting blood samples were 1.7 and 1.29 mmol L^{-1}, respectively, corresponding to optimal fasting TG levels [46], and corresponding concentrations of submicron plasma particles, detected by the SFC, were 3 and 2.1×10^{10} L^{-1}. In the postprandial blood TG level was expectedly higher—3.06 mmol L^{-1}, while concentration of submicron plasma particles increased by 2 orders of magnitude and reached 230×10^{10} L^{-1}, thus, indicating their origin as CMs.

Lipolysis of CMs was initiated in vitro by mixing the postprandial plasma containing CMs with LPL-rich postheparin plasma as described in Section 2. The CM-LPL mixture was further incubated at $T = 37°C$, and CMs were analyzed by the SFC after 10, 30, 55 and 80 minutes of the incubation. Dot-density maps of RI vs size for the intact and lipolyzed CMs in the plasma samples are shown in Figure 3. The dynamics of parameters of corresponding size and RI distributions of CMs larger than 300 nm, namely scale parameter δ and mean RI, are shown in Figure 4A,B, respectively, along with the dynamics of the concentration (Figure 4C). The CM characteristics remain almost the same during the first 10 minutes of the incubation. This may be connected with the primary action of the LPL on smaller (not observed) fraction of CMs. For the next 20 minutes lipolytic activity of the LPL is mainly manifested by the decrease of both the CM concentration and their mean RI, indicating that CMs become less dense due to the loss of their TG content. Thirty minutes after the mixing the CM concentration reach minimal value and remain at this level for the rest of the observation.

Scale parameter δ, on the contrary, keeps constant value of 36 ±2 nm during the first 30 minutes of the CM incubation with the postheparin plasma and sharply rises afterward, reaching the value of 136 ±8 nm at 80 minutes, whereas mean RI keeps decreasing down to 1.4614 ±0.0013. The latter can be interpreted by larger CMs losing their TG from inside and becoming more porous (less dense) in accordance with electron microscopy observations [47, 48]. This hypothesis is additionally supported by deteriorating accuracy of characterization of single CMs (Figure S1), which indicates the accumulated deviations of shape of partly lipolyzed CMs from an ideal homogenous sphere. Interestingly, the size-RI map of CMs after 80 minutes (Figure 3E) already resembles that in fasting plasma (Figure 1A).

3.4 | Postprandial dynamics of CMs in blood

We also observed postprandial dynamics of CMs in blood plasma of a healthy volunteer during 5 hours after consumption of a high-fat breakfast. CMs were analyzed every 30 minutes by the SFC and total plasma TG levels were measured every hour by the enzymatic assay. Size-RI dot-density maps of CMs measured in the fasting plasma (immediately before the meal) and in blood samples drawn 0.5, 1, 2, 3 and 4 hours after the meal are shown in Figure 5A-F, depicting gradual accumulation of submicron particles with RI falling within ranges from 1.45 to 1.55 during the first 2 hours and their disappearance afterward. Figure 6 demonstrates postprandial dynamics of characteristics of the measured CM distributions, including scale parameter δ (Figure 6A) and mean RI (Figure 6B). Both characteristics mostly change during the first hour of observation, when residual CMs in fasting plasma are supplemented with CMs newly formed in the intestine. This change is inverted with respect to that observed during the lipolysis (Figure 4A), even the boundary values quantitatively agree. In particular, within the first hour δ decreases from 124 to 42.4 nm (Figure 6A), while mean RI increases from 1.461 to 1.491 (Figure 6B). Afterward the CM size and RI distributions

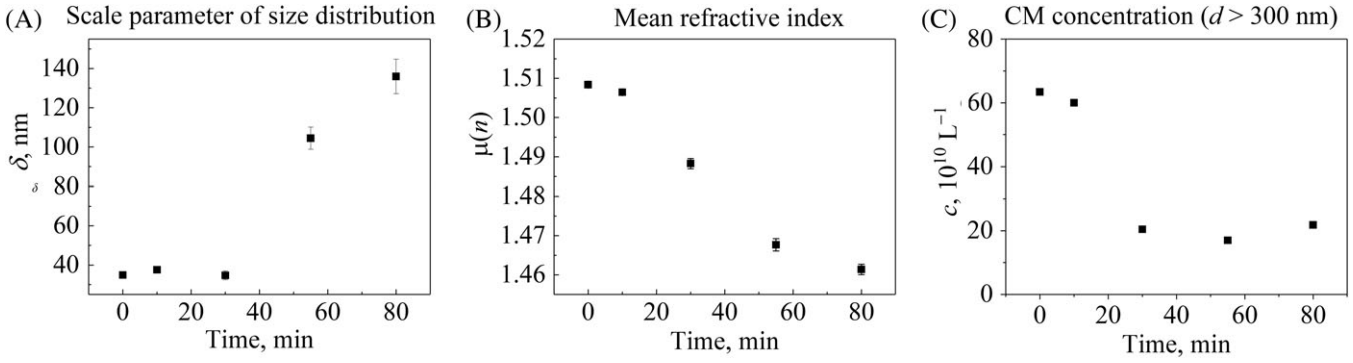

FIGURE 4 Dynamics of CM characteristics during the in vitro lipolysis of CMs in LPL-rich postheparin human plasma for 80 minutes at 37°C: (A) scale parameter δ of the exponential tail of the size distribution; (B) mean RI and (C) concentration of larger CMs (d > 300 nm) in blood plasma

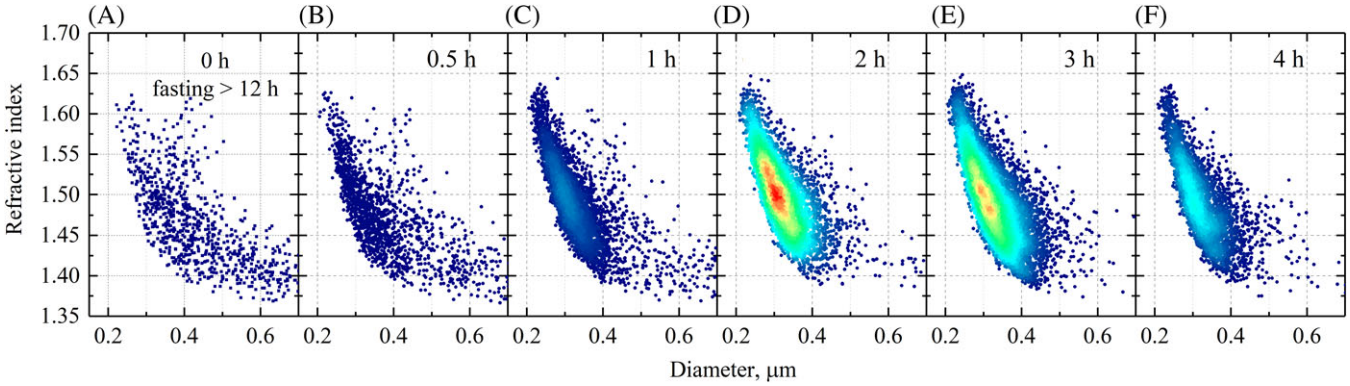

FIGURE 5 Postprandial dynamics of size and RI of CMs in blood plasma. Parts (A) to (F) depict dot-density maps of RI vs. diameter in the fasting blood plasma (0 hour) and 0.5, 1, 2, 3 and 4 hours after the meal, respectively

does not change significantly—both δ and mean RI slightly vary within the ranges 49 ±4 nm and 1.497 ±0.005, respectively.

Postprandial dynamics is then fully described by the dynamics of the CM concentration in blood plasma, according to which CMs accumulate in the bloodstream during 2.5 hours after the meal (20-fold increase in the concentration of CMs larger than 300 nm). During subsequent 1.5 hours the rate of CM synthesis and excretion from the intestine into the blood falls below the rate of their removal, resulting in gradual disappearance of CMs from the bloodstream: CM concentration decrease 4-fold from 2.5 to 4 hours and only slowly afterward (Figure 6C). This sharp fall is quantitatively similar to that during the lipolysis (Figure 4C) albeit at a slower rate due to the continued input of CMs into the bloodstream. Unfortunately, we miss the closure of the cycle, when CM concentration falls to the fasting levels, due to the limited timeframe. Nevertheless, the performed observations generally agree with existing understanding of CM metabolism [5, 6]. They also qualitatively agree with dynamics of total TG in plasma (Figure 6D), although there are 2 apparent differences. First, the dynamic range of TG levels is much smaller. Second, the peak of TG level is shifted and broader. Both are explained by the fact that in addition to TG transported by CMs the total TG level includes TGs circulating in blood as part of other lipids, not detectable by the SFC, mainly CM remnants and VLDL [5].

3.5 | CM characteristics in presence of atherosclerosis

We analyzed fasting blood samples of a healthy volunteer and a patient with atherosclerosis and revealed differences in characteristics of CMs. Corresponding size-RI dot-density maps are shown in Figure 7 and confirm impaired metabolism of CMs for the patient with atherosclerosis (Figure 7B), whose blood contains a greatly elevated number of CMs which have not underwent lipolysis even after a 12-hours fast. Values of δ and mean RI and concentration c of larger CMs detected in blood of the healthy volunteer (Figure 7A) quantitatively agree with that observed in the beginning of

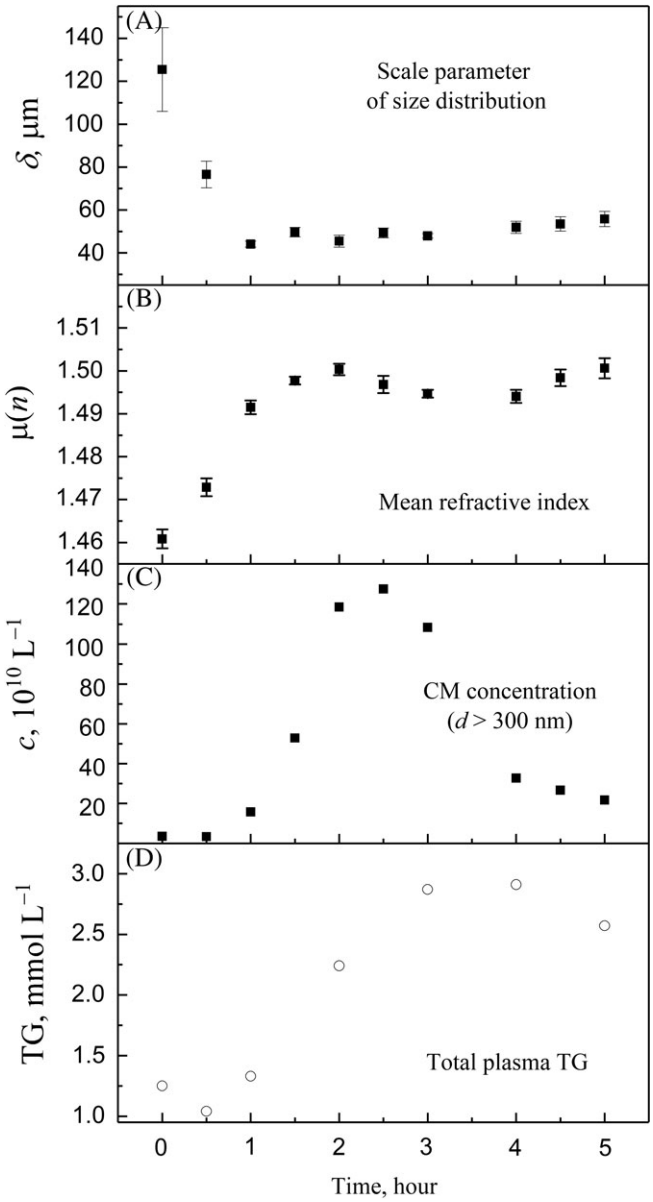

FIGURE 6 (A-C) Postprandial changes of CM characteristics in blood plasma during 5 hours after the meal: the scale parameter δ of the exponential tail of size distribution (A), mean RI (of all detected CMs) (B), concentration of larger CMs (d > 300 nm) (C). (D) Postprandial dynamics of plasma TG levels

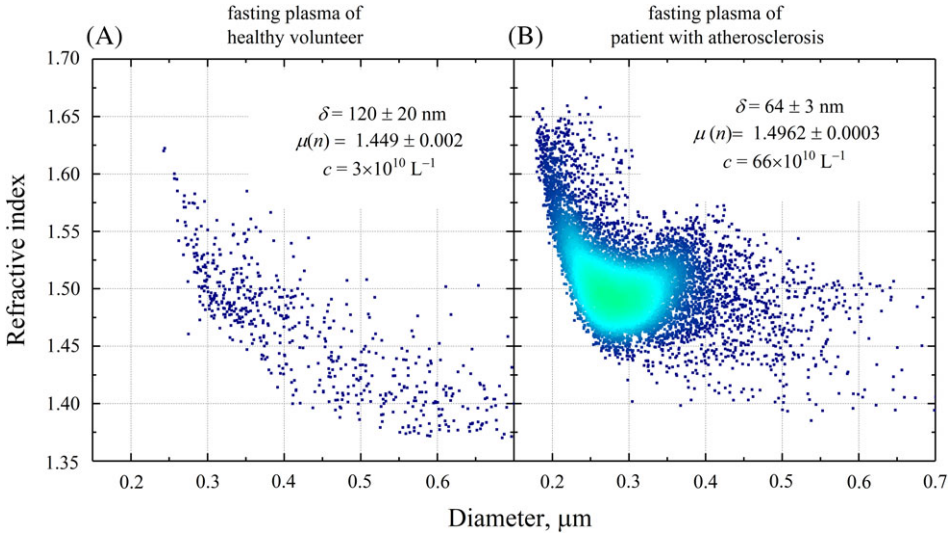

FIGURE 7 Diameter-RI density-dot maps of CMs in fasting plasma of (A) the healthy volunteer (the same as in A) and (B) the patient with atherosclerosis. The corresponding scale parameter δ of the size distribution, mean RI $\mu(n)$ and concentration c of larger CMs ($d > 300$ nm) are also shown (mathematical expectation ± SD)

the CM postprandial dynamics (Figure 6) and by the end of the CM lipolysis (Figure 4, except for c). By contrast, for the patient with atherosclerosis these characteristics agree with that of partly lipolyzed CMs in vitro (between 10 and 55 minutes in Figure 4) and with that of CMs partly removed from the bloodstream after a meal (approximately after 3.5 hours in Figure 6, except for δ). The observed properties of CMs during atherosclerosis generally agree with the literature data [18, 49], but we leave further study of this phenomenon, including the diagnostics potential, for the future.

4 | CONCLUSION

We have demonstrated the capability of the scanning flow cytometry for analysis of CMs in blood plasma based on the light-scattering characterization of individual particles. Light scatter measurements, performed by the SFC, including angle-resolved LSPs and FSC and SSC intensities, provide sufficient information to identify CMs in platelet-rich plasma and to characterize their morphology assuming the spherical model. The size and RI of each particle is determined with the help of the previously developed solution of the ILS problem.

In this paper, we developed a quantitative method to characterize the whole CM population taking into account the practical sensitivity of the SFC, which detects and characterizes CMs only within a limited range of particle characteristics. In particular, we rigorously calculated the instrument detection function (of size and RI), based on simulation of measured signals for single particle and their probability to pass a given threshold. Based on the analysis of uncertainties of individual measurements, we incorporated an extra requirement of $d > 300$ nm, which implied the size and RI accuracy within 10 nanometers and several thousandths, respectively. The obtained RI distribution was independent of size and well described by a normal distribution with mean value between 1.461 and 1.508 depending on the age (lipolysis level) of CMs. The reconstructed size distribution corresponds to the tail of that for the whole CM population, and could be remarkably well described by the exponential distribution characterized by the scale parameter δ.

We applied the developed method to investigate the changes of CM characteristics during 2 key processes relating to CM metabolism. First, we performed in vitro analysis of CMs undergoing lipolysis by the lipoprotein lipase in postheparin plasma, and, second, we performed a postprandial observation of dynamics of CMs in blood plasma of the healthy donor during 5 hours after the high-fat meal. The results of individual particle characterization and estimated parameters of size and RI distributions are consistent with each other and adequately reflect the expected changes. Especially informative is the parameter δ, which showed drastic and reproducible change during lipolysis of freshly produced CMs, both in vitro and in vivo. The corresponding biokinetics model is yet to be developed.

The proposed accurate quantitative characterization of large-size CM subpopulation opens the way for a multitude of medical applications involving screening of CM metabolism. It can be applied both for investigation of the CM role in pathogenesis of different disorders and as a diagnostic tool to reveal diseases caused by or related to the disorders of CM metabolism. The major factor for success of these applications is that the concentration of large-size CMs varies at least 100 times due to physiological conditions, much larger than the corresponding variation of total TG content. This has been exemplified in this paper by differences revealed in the CM characteristics of the healthy volunteer and the patient with atherosclerosis, which potentially can be used for diagnosis and investigation of this dangerous disease.

ACKNOWLEDGMENT

This work was supported by Russian Science Foundation (grant no. 17-75-20117).

REFERENCES

[1] A. M. Gotto, H. J. Pownall, R. J. Havel, *Methods Enzymol.* **1986**, *128*, 3.
[2] W. J. Lossow, F. T. Lindgren, J. C. Murchio, G. R. Stevens, L. C. Jensen, *J. Lipid Res.* **1969**, *10*, 68.
[3] D. E. Vance, J. E. Vance Eds., *Biochemistry of Lipids, Lipoproteins and Membranes*, Elsevier, Amsterdam, The Netherlands **2008**.
[4] K. N. Frayn, Metabolic Regulation: A *Human Perspective*, (Wiley-Blackwell Pub, Chichester, UK, **2010**).
[5] K. Nakajima, T. Nakano, Y. Tokita, T. Nagamine, A. Inazu, J. Kobayashi, H. Mabuchi, K. L. Stanhope, P. J. Havel, M. Okazaki, M. Ai, A. Tanaka, *Clin. Chim. Acta* **2011**, *412*, 1306.
[6] S. S. Gropper, *Advanced Nutrition and Human Metabolism*, Cengage Learning, Belmont, OH **2012**.
[7] J. C. Cohen, *Am. J. Clin. Nutr.* **1989**, *49*, 306.
[8] F. Karpe, T. Olivecrona, A. Hamsten, M. Hultin, *J. Lipid Res.* **1997**, *38*, 949.
[9] H. Yassine, *Lipid Management: From Basics to Clinic*, Springer International Publishing, Switzerland, **2015**.
[10] R. A. Hegele, *Nat. Rev. Genet.* **2009**, *10*, 109.
[11] C. Couillard, N. Bergeron, A. Pascot, N. Alméras, J. Bergeron, A. Tremblay, D. Prud'homme, J.-P. Després, *Am. J. Clin. Nutr.* **2002**, *76*, 311.
[12] A. T. Y. Wong, D. C. Chan, J. Pang, G. F. Watts, P. H. R. Barrett, *J. Clin. Endocrinol. Metab.* **2014**, *99*, E122.
[13] M. Kinoshita, H. Ohnishi, T. Maeda, N. Yoshimura, Y. Takeoka, D. Yasuda, J. Kusano, Y. Mashimo, S. Saito, K. Shimamoto, T. Teramoto, *J. Atheroscler. Thromb.* **2009**, *16*, 517.
[14] M. G. Wilhelm, A. D. Cooper, *J. Atheroscler. Thromb.* **2003**, *10*, 132.
[15] K. J. Williams, I. Tabas, *Arterioscler. Thromb. Vasc. Biol.* **1995**, *15*, 551.
[16] K. M. Botham, E. Bravo, J. Elliott, C. P. D. Wheeler-Jones, *Curr. Pharm. Des.* **2005**, *11*, 3681.
[17] S. Parthasarathy, *Arterioscler. Thromb. Vasc. Biol.* **2010**, *30*, 5.
[18] G. H. Tomkin, D. Owens, *Int. J. Vasc. Med.* **2011**, *2012*, e784536.
[19] S. McNeely, K. Seatter, J. Yuhaniak, M. L. Kashyap, *Clin. Chem.* **1981**, *27*, 731.
[20] G. L. Mills, P. A. Lane, P. K. Weech, *A Guidebook to Lipoprotein Techniques*, Elsevier, Amsterdam, The Netherlands, **1984**.
[21] G. Bucolo, H. David, *Clin. Chem.* **1973**, *19*, 476.
[22] A. M. Lorec, C. Juhel, Y. Pafumi, H. Portugal, A. M. Pauli, D. Lairon, C. Defoort, *Clin. Chem.* **2000**, *46*, 1638.
[23] N. Sakai, Y. Uchida, K. Ohashi, T. Hibuse, Y. Saika, Y. Tomari, S. Kihara, H. Hiraoka, T. Nakamura, S. Ito, S. Yamashita, Y. Matsuzawa, *J. Lipid Res.* **2003**, *44*, 1256.
[24] S. H. Gage, P. A. Fish, *Am. J. Anat.* **1924**, *34*, 1.
[25] H. Ruf, B. J. Gould, Proc. SPIE 2982, Optical Diagnostics of Biological Fluids and Advanced Techniques in Analytical Cytology, **1997**, p. 206.
[26] H. Ruf, B. J. Gould, *Eur. Biophys. J.* **1999**, *28*, 1.
[27] Y. Park, W. J. Grellner, W. S. Harris, J. M. Miles, *Am. J. Physiol.* **2000**, *279*, E1258.
[28] T. Porsgaard, J. Kánskỳ, S. Mason, H. Mu, *Lipids* **2005**, *40*, 273.
[29] A. Werner, *AJP Gastrointest. Liver Physiol.* **2006**, *290*, G1177.
[30] D. Mahl, J. Diendorf, W. Meyer-Zaika, M. Epple, *Colloids Surf. A Physicochem. Eng. Asp.* **2011**, *377*, 386.
[31] H. Lange, *Part. Part. Syst. Charact.* **1995**, *12*, 148.
[32] C. F. Bohren, D. R. Huffman, *Absorption and Scattering of Light by Small Particles*, Wiley, New York, USA, **1983**.
[33] V. P. Maltsev, *Rev. Sci. Instrum.* **2000**, *71*, 243.
[34] D. I. Strokotov, A. E. Moskalensky, V. M. Nekrasov, V. P. Maltsev, *Cytom. Part J. Int. Soc. Anal. Cytol.* **2011**, *79*, 570.
[35] D. I. Strokotov, M. A. Yurkin, K. V. Gilev, D. R. van Bockstaele, A. G. Hoekstra, N. B. Rubtsov, V. P. Maltsev, *J. Biomed. Opt.* **2009**, *14*, 064036.
[36] A. E. Moskalensky, M. A. Yurkin, A. I. Konokhova, D. I. Strokotov, V. M. Nekrasov, A. V. Chernyshev, G. A. Tsvetovskaya, E. D. Chikova, V. P. Maltsev, *J. Biomed. Opt.* **2013**, *18*, 17001.
[37] K. V. Gilev, M. A. Yurkin, E. S. Chernyshova, D. I. Strokotov, A. V. Chernyshev, V. P. Maltsev, *Biomed. Opt. Express* **2016**, *7*, 1305.
[38] A. I. Konokhova, D. N. Chernova, A. E. Moskalensky, D. I. Strokotov, M. A. Yurkin, A. V. Chernyshev, V. P. Maltsev, *Cytometry A* **2016**, *89*, 159.
[39] A. I. Konokhova, D. N. Chernova, D. I. Strokotov, A. A. Karpenko, A. V. Chernyshev, V. P. Maltsev, M. A. Yurkin, *J. Biomed. Opt.* **2016**, *21*, 115003.
[40] M. Cantero, J. R. Conejo, T. Parra, A. Jiménez, F. Carballo, G. de Arriba, *Thromb. Res.* **1998**, *91*, 49.
[41] Y. Yuana, R. I. Koning, M. E. Kuil, P. C. N. Rensen, A. J. Koster, R. M. Bertina, S. Osanto, J. Extracell, *Vesicles* **2013**, *2*, 21494.
[42] N. Arraud, R. Linares, S. Tan, C. Gounou, J.-M. Pasquet, S. Mornet, A. R. Brisson, *J. Thromb. Haemost.* **2014**, *12*, 614.
[43] A. I. Konokhova, M. A. Yurkin, A. E. Moskalensky, A. V. Chernyshev, G. A. Tsvetovskaya, E. D. Chikova, V. P. Maltsev, *J. Biomed. Opt.* **2012**, *17*, 057006.
[44] P. H. Green, R. M. Glickman, *J. Lipid Res.* **1981**, *22*, 1153.
[45] T. H. Gouw, J. C. Vlugter, *Fette Seifen Anstrichm.* **1966**, *68*, 544.
[46] M. Miller, N. J. Stone, C. Ballantyne, V. Bittner, M. H. Criqui, H. N. Ginsberg, A. C. Goldberg, W. J. Howard, M. S. Jacobson, P. M. Kris-Etherton, T. A. Lennie, M. Levi, T. Mazzone, S. Pennathur, *Circulation* **2011**, *123*, 2292.
[47] E. J. Blanchette-Mackie, R. O. Scow, *J. Cell Biol.* **1973**, *58*, 689.
[48] E. J. Blanchette-Mackie, R. O. Scow, *Anat. Rec.* **1976**, *184*, 599.
[49] P. Benlian, J. L. De Gennes, L. Foubert, H. Zhang, S. E. Gagné, M. Hayden, N. Engl, *J. Med.* **1996**, *335*, 848.

SUPPORTING INFORMATION

Additional Supporting Information may be found online in the supporting information tab for this article.

FIGURE S1 Typical weighted experimental and best-fit Mie theory light-scattering profiles (LSPs) of intact (control) CMs, measured in postprandial plasma, obtained 3 hours after a meal (A and B), and lipolyzed CMs, measured in postprandial plasma 80 minutes after its incubation with LPL-rich postheparin plasma (C and D). Estimates of particle diameter d and RI n are also shown (mathematical expectation $\pm$ SD). Larger uncertainties of characteristics estimates and systematic differences between experimental and best-fit theoretical LSPs for the lipolyzed CMs indicate deviation of their shape from an ideal homogeneous sphere.

FIGURE S2 (A) Typical experimental FSC signal and the 1 simulated for CM with size $d = 300$ nm and RI $n = 1.462$. The calculated probability to detect this CM for the specified threshold level is 0.92. (B) 3D representation of the SFC detection function (the probability to detect a single microsphere) versus its size and RI in the range from 100 to 600 nm and from 1.35 to 1.7, respectively.

FIGURE S3 Variation of the SFC detection efficiency due to the experimental conditions. Blue and red curves represent constant levels of detection probability of 0.1 and 1 for observations of CM lipolysis (solid lines) and observations of postprandial dynamics (dashed lines), respectively.

FIGURE S4 Uncertainties of size (A) and RI (B) estimates of individual CMs during observations of CM lipolysis (gray

bars) and observations of CM's postprandial dynamics (dashed bars). Both samples were collected 3 hours after the meal (before mixing with the LPL-rich plasma), thus the differences are mostly due to different experimental conditions (but also due to different donors).

FIGURE S5 Size-dependent detection probability function $F_{det}(d)$ determined for each time sample during observations of CM lipolysis (A) and CM postprandial dynamic (B). Decrease of the detection efficiency with time is caused by shifting of the whole CM distributions over RI to lower values.

FIGURE S6 Apparent CM size distributions (gray bars), measured after 0 (A) and 55 minutes (B) of CM incubation with LPL-rich plasma ($d > 300$ nm). Reconstructed CM size distributions (red bars) are obtained by dividing experimental ones by corresponding detection probability function $F_{det}(d)$ (see Figure S5A) and fitted by exponential distribution (black line) to determine the scale parameter δ.

FIGURE S7 (A) Exponential decay of the reconstructed size distribution of CMs, measured in postprandial plasma. The tail for sizes greater than 300 nm (dots) is well described by the exponential distribution (red line). (B) Attempt to fit the same tail by the gamma distribution (red solid line), showing also the small-size (extrapolated) part (red dashed line). Incorporating additional distribution parameter τ causes loss of the accuracy of δ, while the extrapolated part of the distribution (including its mode) is not reliable, since the 95% confidence band (gray hairlines shown only for $d < 300$ nm) is very broad. In both parts the fitted values of distribution parameters are shown as mathematical expectation $\pm$ SD.

How to cite this article: Chernova DN, Konokhova AI, Novikova OA, et al. Chylomicrons against light scattering: The battle for characterization. *J. Biophotonics*. 2018;11:e201700381. https://doi.org/10.1002/jbio.201700381